Journal of Power Sources 263 (2014) 29–36

Contents lists available at ScienceDirect

Journal of Power Sources

journal homepage: www.elsevier.com/locate/jpowsour

Influence of the porosity degree of poly(vinylidene fluoride-*co*-hexafluoropropylene) separators in the performance of Li-ion batteries

R.E. Sousa [a], J. Nunes-Pereira [a], C.M. Costa [a], M.M. Silva [b], S. Lanceros-Méndez [a,*], J. Hassoun [c], B. Scrosati [c,d], G.B. Appetecchi [c,*]

[a] Centro/Departamento de Física, Universidade do Minho, 4710-057 Braga, Portugal
[b] Centro/Departamento de Química, Universidade do Minho, 4710-057 Braga, Portugal
[c] Chemistry Department, University of Rome "La Sapienza", P.le A. Moro 5, 00185 Rome, Italy
[d] Helmholtz Institute, Ulm, Germany

HIGHLIGHTS

- The effect of porosity degree in P(VdF–HFP) membranes is investigated.
- Correlation among porosity, liquid uptake, tortuosity and conductivity is established.
- Room temperature conductivity above 10^{-3} S cm^{-1} is obtained for the 5/95 sample.
- From 70% to 90% of the theoretical capacity is delivered by Li/Sn–C and Li/LiFePO4 half-cells.
- A charge/discharge efficiency close to 100% is observed in Li/Sn–C and Li/LiFePO4 half-cells.

ARTICLE INFO

Article history:
Received 10 November 2013
Received in revised form
27 March 2014
Accepted 7 April 2014
Available online 15 April 2014

Keywords:
Porous membranes
Polyvinylidenedifluoride
–hexafluoropropylene
P(VdF–HFP)
Lithium batteries

ABSTRACT

Polyvinylidenedifluoride–hexafluoropropylene, (P(VdF–HFP))-based polymer electrolytes, as separators for lithium batteries, were prepared through different polymer/solvent (*N*,*N*-dimethylformamide, DMF) ratios and physicochemically investigated. Scanning electron microscopy measurements have shown a homogeneously distributed porosity within the membranes, with moderately tortuous pathways, resulting in a liquid uptake up to 77 wt.% with respect to the overall weight and conduction values above 10^{-3} S cm^{-1} at room temperature.

Prolonged cycling tests, performed on Li/Sn–C and Li/$LiFePO_4$ half-cells based on P(VdF–HFP) polymer electrolyte separator membranes, have evidenced nominal capacities ranging from 70% to 90% of the theoretical value with very good capacity retention and charge/discharge efficiency close at 100% even at high current rates. A capacity decay is observed at high current regime, associated to the diffusion phenomena occurring within the electrode and the polymer electrolyte separator membrane.

1. Introduction

In the last decade, rapid developments in electronics miniaturization and novel portable electric devices technologies [1,2] led to strongly increasing needs of safe and high density energy storage devices, focusing in particular on rechargeable lithium ion batteries [1,3]. Recently, lithium ion battery systems have been expanding for other applications such as aerospace technologies, electric and hybrid vehicles [4].

Liquid electrolytes currently used in commercial lithium-ion *batteries are based on* organic solvents (mainly alkyl carbonates), which are volatile, flammable and easy to ignite on exposure to high temperatures [5]. Gel polymer electrolytes (GPEs), e.g., formed by a liquid solution trapped through a polymer host, are receiving considerable attention as lithium battery solid separators [6,7] due to their simple processability, feasibility to suit various cell geometries, cost competitiveness and safety [3] in combination with ionic conduction comparable to the one of the most used liquid electrolytes, low density, mechanical flexibility and stability [6–8].

* Corresponding authors.
E-mail addresses: lanceros@fisica.uminho.pt (S. Lanceros-Méndez), gianni.appetecchi@enea.it, gianni.appetecchi@alice.it (G.B. Appetecchi).

http://dx.doi.org/10.1016/j.jpowsour.2014.04.014
0378-7753/

In the last years, various polymer hosts with different chemical structures have been investigated [1–8]. Among these, PVdF and its copolymers have been chosen as potentially interesting hosts by virtue of their appealing properties [9] such as high solubility in dispersed media, low crystallinity degree, low glass transition temperature, high dielectric constant (able to assist ionization of lithium salts), possibility of tuning the separator porosity degree and pore size (through binary and ternary polymer/solvent systems), good contact at electrolyte/electrode interface and stability in cathodic environment [8].

Among PVdF-based copolymers, the Polyvinylidenedifluoride–hexafluoropropylene (P(VdF–HFP)) material has drawn great attention [1] as polymer host for lithium ion battery GPEs. The incorporation of hexafluoropropylene (HFP) amorphous phases into vinylidene fluoride (VdF) blocks is able to modify the properties of the homopolymer, e.g., promoting the uptake of larger liquid electrolyte contents [9,10] and enhancing the flexibility of the polymer chains (and thus enabling the assisted transport of the lithium cations [11]), whereas the crystalline VdF phase provides sufficient mechanical integrity for processing free-standing films [10]. The pore size and shape, the volume fraction and interconnectivity of the pores are key factors for determining the retention ability and, therefore, the ionic conductivity of GPEs [12].

Many techniques have been developed for the preparation of porous polymer electrolyte membranes such as preferential dissolution, immersion precipitation method, template-leaching technique, evaporation phase inversion, melt spinning and cold stretching, thermally induced phase separation (TIPS) and liquid–liquid extraction process [13]. In order to explore the optimum condition for the pore generation, P(VdF–HFP)-based polymer electrolytes were also prepared through different solvent/non-solvents combinations [13] and immersion precipitation [13]. Polymer hosts with large pore size and high porosity can be obtained by adding additives, e.g., polyvinylpyrrolidone (PVP), polyethyleneglycol (PEG), can be dissolved in the casting solution [12].

The objective of the present work is to establish a correlation among the microstructure (e.g., pore size and porosity degree) of the P(VdF–HFP) membranes, prepared through binary polymer/solvent (*N*,*N*-dimethylformamide, DMF) systems, and their properties for battery applications such as electrolyte solution uptake and ionic conductivity. P(VdF–HFP) films, obtained from polymer/solvent slurries having different weight compositions, were prepared and investigated. The performance of the polymer electrolyte membranes as a function of the porosity degree was evaluated in Li/$LiFePO_4$ and Li/Sn–C half-cells. The results are reported in the present manuscript.

2. Experimental

2.1. Materials

Poly(vinylidene fluoride–co-hexafluropropylene), P(VdF–HFP), Solef® 21216 (Solvay, $M_w = 600.000$ Da, VdF–HFP mole ratio equal to 88/12) and lithium bis (trifluoromethanesulfonyl) imide, LiTFSI (Sigma–Aldrich) were dried under vacuum at 25 °C for 48 h and 25 °C for 96 h, respectively. *N*,*N*-dimethylformamide (DMF) and propylene carbonate (PC) were purchased from Merck and used as received.

2.2. Membrane preparation

Appropriate amounts of P(VdF–HFP) were added to DMF to prepare solutions having polymer/solvent weight ratio equal to of 5/95, 10/90, 15/85 and 20/80, respectively. The solutions were prepared at room temperature by stirring the two components until complete polymer dissolution. The solutions were then cast on clean glass substrates and spread by blade coating to obtain membranes ranging from 30 to 75 μm. Finally, the full removal of the DMF solvent was allowed by drying in an oven at 25 °C for 24 h.

2.3. Morphological characterization of the P(VdF–HFP) membranes

The morphology of the polymer membranes was analyzed using a scanning electron microscopy (SEM, Cambridge, Leica) with an accelerating voltage of 3 kV. The membrane samples were previously coated with a thin gold layer using a sputter coating (Polaron, model SC502 sputter coater). The average pore diameter was determined on the basis of the diameter of 40 different pores, using the SEM images at 200× magnification and the Image J software. Membrane porosity was determined through density measurements using a pycnometer in according to Eq. (1) [14]:

$$\rho_m = \frac{\rho_w m_3}{m_1 + m_3 - m_2} \quad (1)$$

where ρ_m represents the density of the membrane sample (the density of the pristine polymer, ρ_{pol}, is equal to 1.77 g cm^{-3}), ρ_w is the water density, m_1 is the mass of pycnometer with water, m_2 is the mass of pycnometer with water and the membrane and m_3 is the mass of the dry membrane. The porosity (φ) was calculated according to Eq. (2) [14]:

$$\phi = 1 - \frac{\rho_m}{\rho_{pol}} \quad (2)$$

The tortuosity (τ) of the electrolyte membrane conduction pathways (pores), e.g., the ratio between the thickness sample and the effective pore length, was determined by the relation:

$$\tau = \sqrt{\frac{\sigma_0 \phi}{\sigma_i}} \quad (3)$$

where σ_0 is the conductivity of the liquid electrolyte and σ_i and φ represent the conductivity and the porosity of the membrane, respectively.

2.4. Liquid electrolyte uptake

The electrolyte uptake was determined by immersing the membranes in a solution of 1 M LiTFSI in PC, i.e., showing a conductivity (σ_0) equal to 6.5×10^{-3} S cm^{-1} at 25 °C, for 24 h. The electrolyte content ($E_{content}$) was evaluated according to:

$$E_{content} = \left(1 - \frac{m_0}{m_E}\right) \times 100 \quad (4)$$

where m_0 is the mass of the dry membrane and m_E is the mass of the membrane upon loading with electrolyte solution.

2.5. Physicochemical characterization

Polymer phase in the membranes was investigated by Fourier Transformed Infrared (FTIR) spectroscopy (Perkin–Elmer, model 1610) at room temperature using a Jasco FT/IR-4100. FTIR spectra were collected in ATR mode from 4000 to 600 cm^{-1} after 32 scans with a resolution of 4 cm^{-1}.

The thermal properties of the membranes were determined by differential scanning calorimetry (DSC) with a Mettler Toledo 821^e apparatus. The samples were punched from the central region of membranes, placed in 50 μL crucibles and heated from 50 to 200 °C at a rate of 10 °C min^{-1} under a nitrogen atmosphere. The crystallinity

degree (χ_c) was calculated from the peak enthalpy (ΔH_f) based on the enthalpy of a 100% crystalline sample ($\Delta H_{100-\beta} = 103.4\ J\ g^{-1}$):

$$\chi_C = \frac{\Delta H_f}{\Delta H_{100}} \times 100 \quad (5)$$

2.6. Transport properties

The ionic conductivity was evaluated by impedance spectroscopy, using an Autolab PGSTAT-12 (Eco Chemie) set-up, in a frequency range from 65 kHz through 500 mHz. The samples were housed within symmetrical two gold blocking electrode cells located in a Buchi TO50 oven. The measurements were performed within an argon filled glove box in a temperature (controlled by a type K thermocouple) range from 20 °C to 120 °C by heating scans at 8 °C h^{-1}. The ionic conductivity (σ_i) was calculated according to Eq. (6):

$$\sigma_i = \frac{d}{R_b A} \quad (6)$$

where R_b represents the electrolyte membrane bulk resistance, obtained by impedance spectroscopy, d is the thickness of the electrolyte sample and A is the electrochemical active area, respectively.

2.7. Lithium cell manufacturing and testing

The Sn–C anode active material, e.g., formed by tin nanoparticles uniformly dispersed in a micrometric carbon matrix with an Sn:C weight ratio equal to 3:7, was prepared as described in previous papers [15–18] with a tin content of about 35% corresponding to a theoretical capacity equal to 400 mA h g^{-1}. The $LiFePO_4$ cathode material, displaying a theoretical specific capacity of 170 mA h g^{-1}, is a commercial product (Model A1100, LFP-NCO product line) developed and manufactured by Advanced Lithium Electrochemistry (Aleees Taiwan) [17].

Composite electrodes were prepared by blending the active material (Sn–C or $LiFePO_4$), the electronic conductor (Super-P carbon, MMM) and the binder (PVdF, Solvay) in *N*-methyl-pyrrolidone. The so-obtained slurry was cast onto copper (Sn–C) or aluminum ($LiFePO_4$) foil, allowing the solvent removal. Coin electrodes, having a 10 mm diameter and thickness ranging from 40 μm to 50 μm, were punched from the tapes. Finally, the electrodes were dried under vacuum at 110 °C overnight and transferred in the glove box. The weight composition of electrodes resulted 80(active material):10 (electronic conductor):10(binder) with an active material mass loading of 2.0 mg cm^{-2} (anodes) and 4.0 mg cm^{-2} (cathodes), corresponding to 0.8 mA h cm^{-2} (Sn–C anodes) and 0.68 mA h cm^{-2} ($LiFePO_4$ cathodes), respectively.

The Li/Sn–C and Li/$LiFePO_4$ half-cells were fabricated by housing in 2032 coin-type containers the sequence composed by a lithium disc anode (10 mm diameter), a swollen P(VdF–HFP)-based electrolyte membrane (14 mm) and an Sn–C (or $LiFePO_4$) electrode (10 mm). The cycling performance of the half-cells was evaluated using a multichannel Maccor 4000 battery tester at room temperature. The (galvanostatic) measurements were performed within the 0.01–2.0 V (anode half-cells) and 2.5–4.0 V (cathode half-cells) voltage range, respectively, at current rates from 0.1 C (40 mA g^{-1} and 17 mA g^{-1} for the Sn–C and the $LiFePO_4$ electrode, respectively) through 2 C (0.8 A g^{-1} and 0.34 mA g^{-1}).

3. Results and discussion

The above described procedure route allowed to obtain homogenous P(VdF–HFP) separator membranes having good mechanical properties and thickness ranging from 80 to 120 μm. Membranes prepared from slurries having a P(VdF–HFP)/DMF weight ratio equal to 5/95 resulted in white colored samples whereas an increase of the polymer/solvent ratio up to 20/80 gives translucid appearance.

3.1. Microstructural characteristics

The membrane morphology strongly affects the performance of the battery as well as the assembly process. Fig. 1 shows the cross section SEM image of P(VdF–HFP) separator membranes obtained from slurries having different polymer/solvent weight ratios. The porosity of the P(VdF–HFP) membranes is the result of the polymer–solvent (DMF) interaction in the phase diagram of binary systems [19] and might be explained as a liquid–liquid phase separation and consequent crystallization of the copolymer rich phase [20]. The presence of open and homogeneously distributed porosity with interconnected pathways is well evidenced in the membranes, particularly in samples 5/95 (panel a) and 10/90 (panel b). A further increase of the polymer fraction within the slurry prepared for obtaining the separator membranes leads to a decrease in porosity content and pore size as shown in panels c (sample 15/85) and d (sample 20/80). Therefore, optimal P(VdF–HFP) separator membranes can be obtained from polymer/DMF slurries with a solvent content equal or above to 90% in weight.

Fig. 2 reports the porosity and electrolyte content trend of P(VdF–HFP) separator membranes obtained from slurries having different polymer/solvent weight ratios. It is observed a generally decreasing liquid uptake (solid squares) with increasing polymer content in the starting slurry. The solution (e.g., LiTFSI in PC) content ranges from 76% to 77% (in weight) for polymer fractions equal or below 10% in weight whereas further increase of the P(VdF–HFP) content leads to a sharp decrease of the liquid uptake down to 26–32%. However, this does not seem to be in good agreement with the trend exhibited by the porosity (open squares). For instance, a liquid uptake decrease from 32% to 26% (in volume) is observed by passing from a polymer weight fraction of 0.15–0.20, despite an increase in porosity from 56% to 70% in volume. This apparently contrasting behavior is likely ascribable to the presence of blind (closed) pores (due to the higher polymer fraction in the P(VdF–HFP)-DMF preparation slurry), which are not filled by the liquid electrolyte and, therefore, do not take part in the uptake process.

The tortuosity (τ) value of these samples is reported in Table 1. The tortuosity gives information about pore connectivity relating the mean actual path with sample thickness and is correlated with the conduction process through ionic conductivity [21]. High τ values indicate longer ionically conductive pathways, resulting in lower ionic conductivity and enhancing diffusive phenomena through the polymer electrolyte. Otherwise, low tortuosity highlights short conduction pathways, this leading to faster ion transport properties and, consequently, to high battery cycling performance and rate capability. The ideal τ value is equal to 1, corresponding to a perpendicular conduction pathway across the polymer electrolyte, which represents the optimal condition for assuring high conduction values. The results of Table 1 indicate a marked tortuosity increase with the polymer fraction in the starting slurry for obtaining the P(VdF–HFP) membrane, this resulting correlated with the porosity degree and pore connectivity. The sample 5/95 shows a τ value equal to 2, which rises up to 16 for the membrane 15/85.

3.2. Physicochemical properties

The results obtained from FT-IR analysis and thermal measurements performed on P(VdF–HFP) membranes are presented in

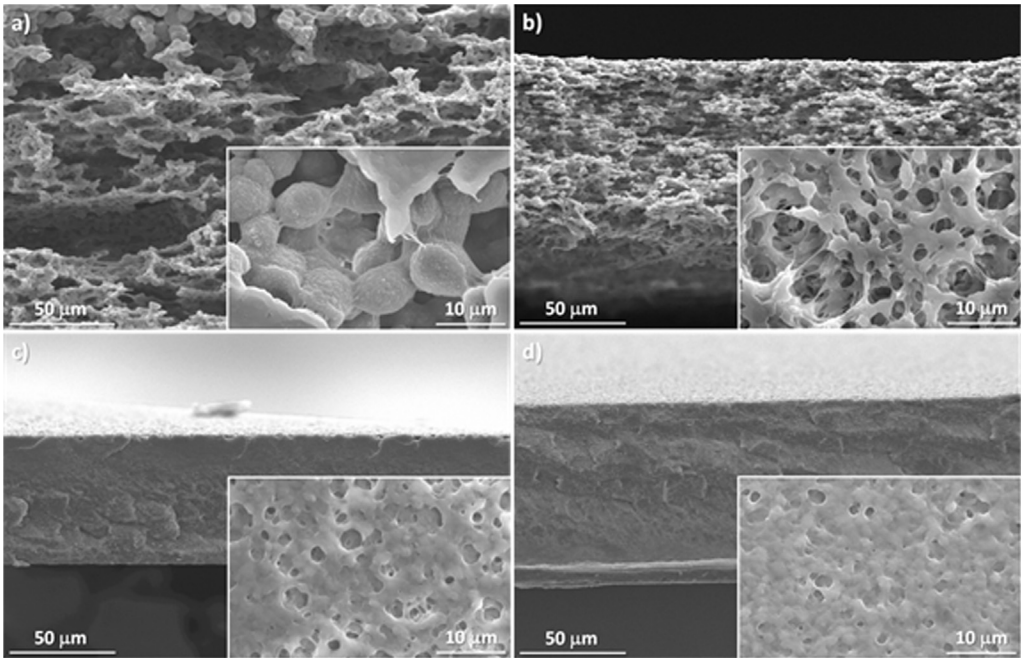

Fig. 1. Cross-section SEM picture of P(VdF–HFP) separator membranes prepared from slurries having different polymer/solvent weight ratios. (a) 5/95. (b) 10/90. (c) 15/85. (d) 20/80. A magnification of the each SEM picture is reported in the inserts.

Fig. 3. The characteristic vibration modes (833 cm^{-1} and 1402 cm^{-1}) of the β-phase crystalline of the P(VdF–HFP) polymer do not change independently on the preparation conditions and porosity degree, indicating that the polymer crystallizes in the same phase [9,22]. The amorphous phase of this copolymer is confirmed by the presence of vibrational band at 874 cm^{-1} [23].

The DSC traces (panel b) highlight an endothermic peak centered at about 140 °C corresponding to the melting of the P(VdF–HFP) copolymer. No relevant difference on the thermal properties was observed with the polymer fraction increase within the starting slurry. The degree of crystallinity (χ_c) for all the samples is presented in Table 1. This parameter is seen to range from 29% to 35%, being therefore independent on the polymer/solvent weight ratio within experimental error.

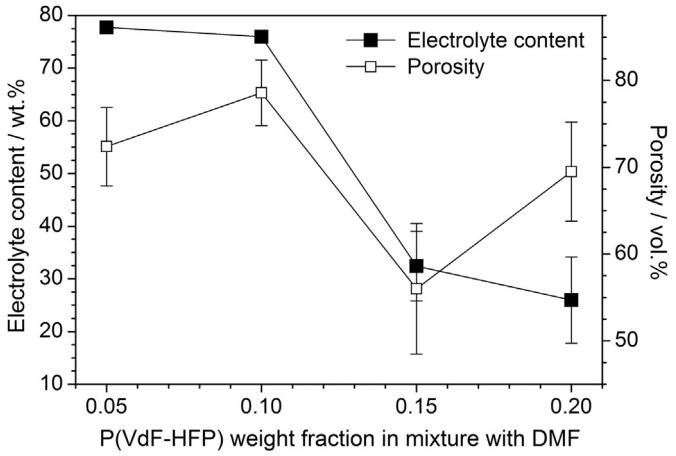

Fig. 2. Liquid uptake and porosity of P(VdF–HFP) separator membranes prepared from slurries having different polymer/solvent weight ratios.

Table 1
Physicochemical properties of P(VdF–HFP) electrolyte membranes obtained through polymer/solvent slurries having different weight compositions.

Electrolyte sample	Porosity (vol.%)	Liquid uptake (wt.%)	Tortuosity	Crystallinity (degree/%)	Conductivity (20 °C)/S cm^{-1}
5/95	72 ± 5	77 ± 1	2	31	$(1.3 \pm 0.1) \times 10^{-3}$
10/90	79 ± 4	76 ± 1	6	29	$(1.4 \pm 0.1) \times 10^{-4}$
15/20	56 ± 7	32 ± 1	16	35	$(1.4 \pm 0.1) \times 10^{-5}$
20/80	70 ± 6	26 ± 1	11	32	$(3.8 \pm 0.1) \times 10^{-5}$

3.3. Transport properties

The transport properties were investigated in terms of ionic conductivity as a function of the temperature, determined by impedance spectroscopy measurements taken on symmetric two gold electrode cells (Au°/electrolyte membrane sample/Au°) at temperature intervals ranging from 20 °C to 120 °C. The room temperature AC responses, represented in Fig. 4a as Nyquist plots, show an inclined straight-line (typical of the blocking electrode capacitive behavior) whose intercept with the real axes, Z′, gives the PVdF-based electrolyte membrane ionic resistance [24,25]. This value was obtained through analysis of the impedance responses, performed using a common approach, i.e., by defining an equivalent circuit taking into account all possible contributions to the impedance of the tested electrolyte membranes [24,25]. The validity of the chosen circuit was confirmed by fitting the impedance responses using a non-linear least-square (NLLSQ) fit software developed by Boukamp [26,27]. Only fits characterized by a χ^2 factor [26,27] lower than 10^{-4} were considerable acceptable to assure the validity of the proposed model. The equivalent circuit, proposed to represent the electrochemical cell under study, is constituted by two elements connected in series, e.g., the electrolyte bulk resistance (R) and the double layer capacitance at electrolyte/electrode interface (Q_{dl}). A constant-phase element, CPE (Q), was used in the place of pure capacitance (C).

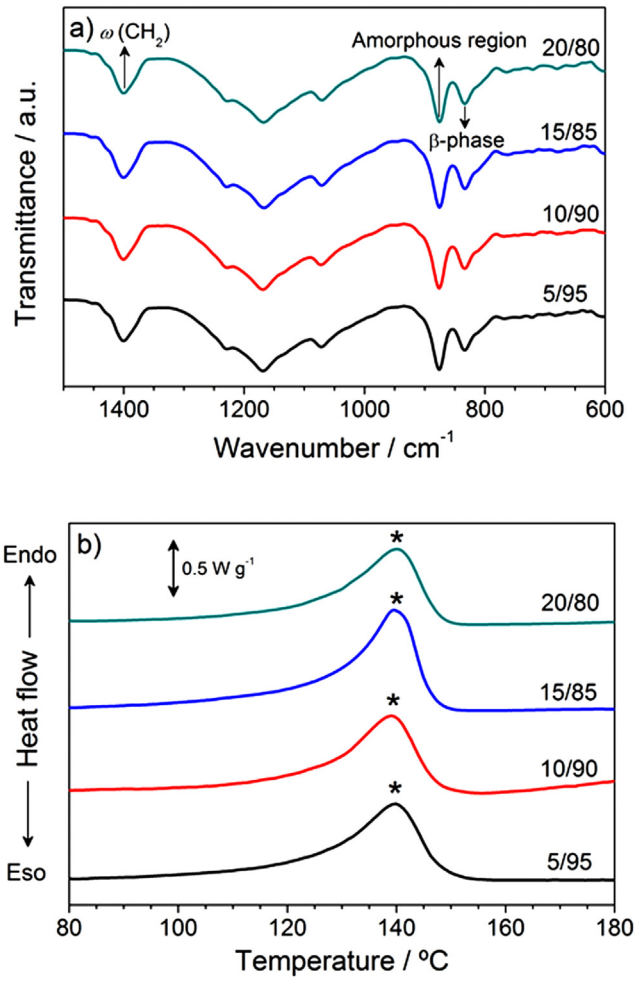

Fig. 3. FT-IR spectrum (a) and DSC trace (b) of P(VdF–HFP) separator membranes prepared from slurries having different polymer/solvent weight ratios.

The ionic conductivity vs. temperature dependence of the P(VdF–HFP)-based electrolyte membranes is plotted in panel b of Fig. 4, which denotes how conduction values above 10^{-3} S cm^{-1} are exhibited at room temperature (below 20 °C) by the 5/95 sample (solid square). An increase of the P(VdF–HFP) fraction above 0.05 (5 wt.%) in the polymer/solvent slurry, prepared for obtaining the separator membranes, leads to a progressive decrease in ionic conduction. Above a polymer fraction equal to 0.10, the conduction values do not exceed 10^{-4} S cm^{-1} even at medium-high temperatures. This issue is in good agreement with the results reported in Fig. 2 and Table 1, which evidence a decay in porosity and liquid uptake and an increase in tortuosity of the ion conduction pathways with increasing the polymer/solvent weight ratio. For instance, the 5/95 polymer electrolyte sample displays the highest conductivity values. Surprisingly, the 20/80 sample exhibits higher conduction values with respect to the 15/85 electrolyte membrane. This behavior may be ascribed to an optimal pore size and interconnection, thus allowing a better distribution of the liquid content. A moderate raise in conductivity is observed with increasing temperature, suggesting that the ion movement is activated by modest energy amounts, as generally expected in gel electrolytes [28–30].

Table 2 compares the physicochemical properties of the polymer electrolyte developed in the frame of this work with those of similar P(VdF–HFP) electrolyte membranes containing different Li^+ conducting, organic solutions as reported in literature [8,31–33].

Table 2
Physicochemical properties of P(VdF–HFP) membranes swollen in different lithium ion conducting, organic solutions. References are reported in the table.

Electrolyte solution	Porosity (%)	Ionic conductivity (S cm^{-1})	Reference
LiTFSI (1 M) – PC	72	1.3×10^{-3}	This work
$LiClO_4$ (1 M) – EC/PC (1/1 w/w)	83	1.5×10^{-3}	[31]
$LiPF_6$ (1 M) – EC/DMC (1/1 w/w)	78	3.4×10^{-4}	[8]
$LiBF_4$ (1 M) – EC/γBL (1/3 w/w)	n.a.	3.4×10^{-3}	[32]
$LiPF_6$ (1 M) – EC/DEC (1/1 w/w)	70–90	1.2×10^{-3}	[33]

The different values of porosity degree depend on the processing techniques whereas the ionic conductivity value is affected by the liquid solution used in the polymer electrolytes. It is to note that the P(VdF–HFP) electrolyte system developed in the present work

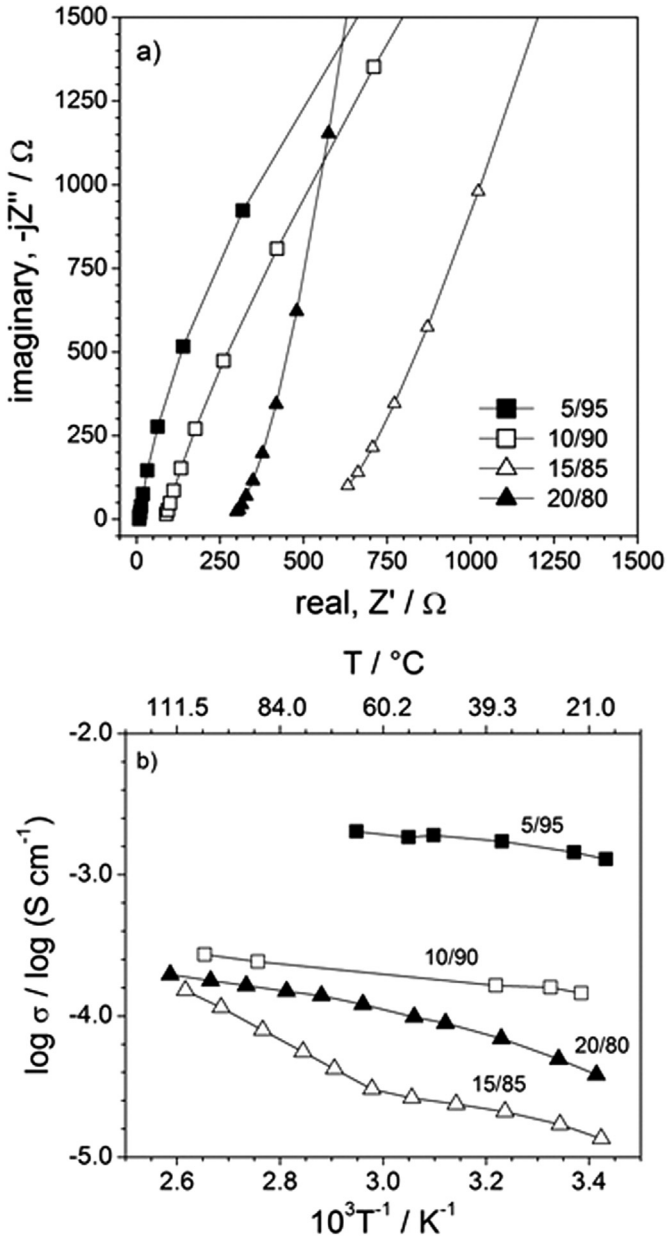

Fig. 4. Room temperature AC response (a) and conductivity Arrhenius plot (b) of polymer electrolytes based on P(VdF–HFP) separator membranes prepared from slurries having different polymer/solvent weight ratios.

exhibits comparable ion conduction value despite a lower porosity degree. This suggests a better pore distribution through the P(VdF–HFP) host ascribable to a good optimization of the solvent/polymer ratio.

3.4. Battery tests

The electrochemical performance of the P(VdF–HFP)-based polymer electrolyte membranes was evaluated in Li/Sn–C and Li/$LiFePO_4$ half-cells. The sample 5/95, showing the best liquid uptake (Fig. 2) and ion-transport properties (Fig. 4), was selected as the preferred ionically conducting separator.

Fig. 5 shows selected voltage vs. capacity profiles obtained upon prolonged cycling tests run on an Li/Sn–C half-cell (panel a). The typical voltage signature of the Sn–C material was displayed, characterized by an initial irreversible capacity, e.g., associated with the electrode structural reorganization, solid electrolyte interface (SEI) film formation [34] and eventual impurities decomposition (reduction), followed by reversible cycles (i.e., lithium–Sn alloying–dealloying [15,17,35]), with average voltage value of about 0.6 V vs. Li/Li^+. A capacity of about 300 mA h g^{-1} was delivered, corresponding to 75% of the theoretical value and approaching the performance observed in liquid electrolytes [15]. Apart the first cycle, the discharge/charge efficiency quickly levels around 100%, highlighting a highly reversible alloying–dealloying process. Prolonged cycling tests (panel b), performed at medium charge/discharge current rate (C/5) and deep of discharge (DoD) equal to 100%, indicate a good capacity retention.

The applicability of the P(VdF–HFP) polymer electrolytes was further studied in lithium cells using $LiFePO_4$ as the working electrode. Fig. 6 shows selected voltage vs. capacity profiles (panel a) obtained upon prolonged cycling tests, run at C/5 and 100% of DoD, on an Li/$LiFePO_4$ cathode half-cell. The voltage profile feature reflects the reversible charge (lithium removal)-discharge (lithium uptake) cycling behavior of $LiFePO_4$ characterized by a flat plateau evolving at around 3.5 V vs. Li/Li^+, with first charge capacity extending up to 180 mA h g^{-1} and reversible capacity during the following cycles of the order of 120 mA h g^{-1} (e.g., 71% of the theoretical value). The irreversible capacity observed during the first charge half-cycle is most likely due to SEI film formation [34] and oxidation of eventual impurities in the electrolyte membrane. The discharge/charge efficiency, apart the initial irreversible capacity, levels at 100% starting from the second cycle for both cathode half-cells. Panel b of Fig. 6 plots the cycling performance obtained a current rate of C/5. The results show a modest capacity fading during cycling tests. For cathodic half-cells, the delivery capacity at 0.1 C is 122.1 mA h g^{-1} (71% of the theoretical value), approaching the one observed in $LiPF_6$-EC-DMC liquid electrolyte supported by glass fiber separators (155 mA h g^{-1} at 0.1 C) [17,18,36].

The half-cells (anodic and cathodic) based on the P(VdF–HFP) 5/95 separator membrane have been selected for further investigation in terms of the rate capability. Fig. 7 reports the voltage vs. capacity profiles (panels a and c) and the capacity evolution (panels

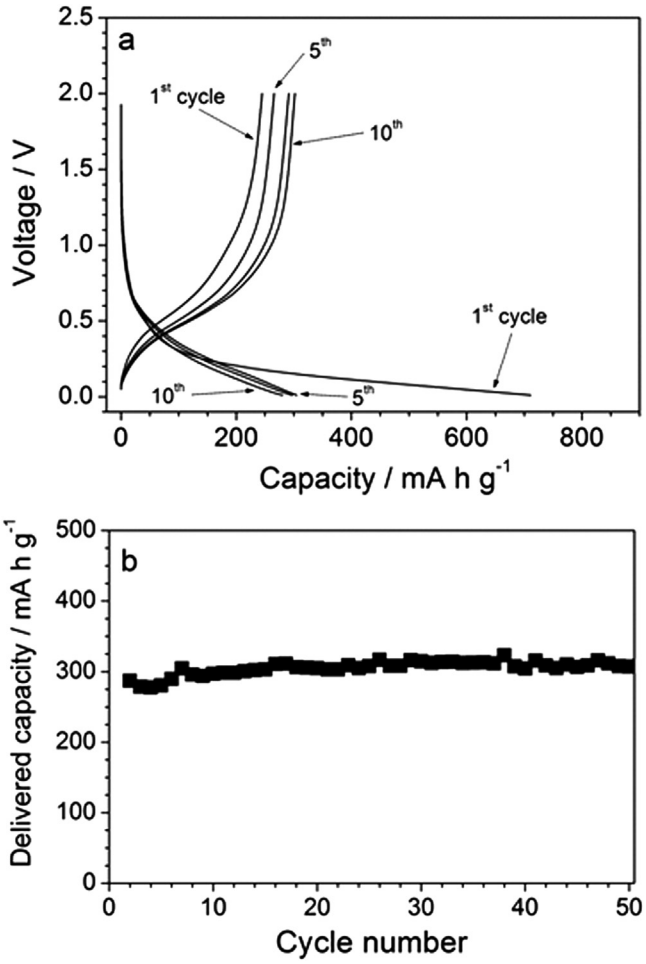

Fig. 5. Selected voltage vs. capacity profiles (a) and cycling performance (b) of an Li/Sn–C anode half-cell using the polymer electrolyte separator membrane 5/95. Current rate: 0.2 C. Room temperature.

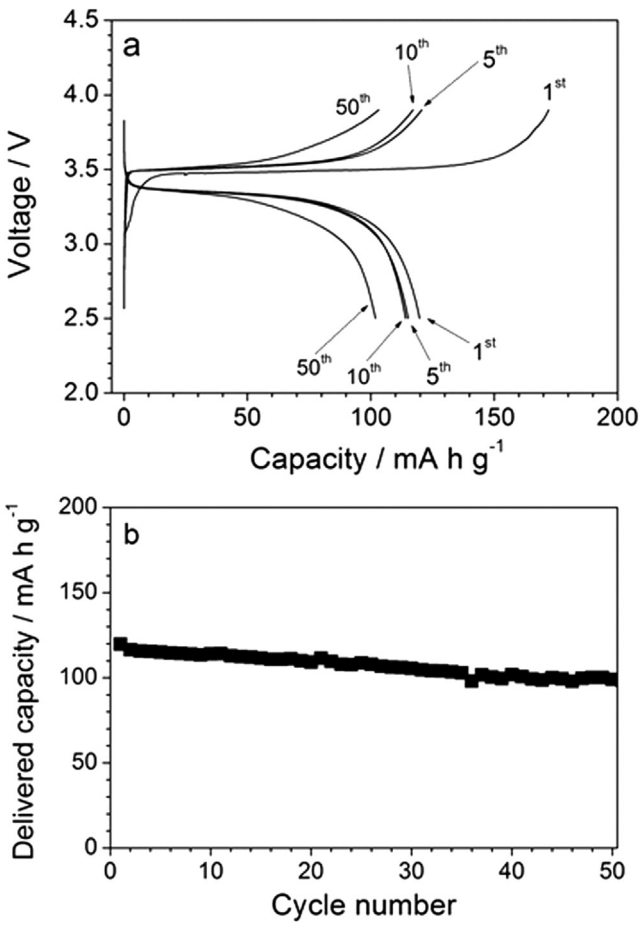

Fig. 6. Selected voltage vs. capacity profiles (a) and cycling performance (b) of an Li/$LiFePO_4$ cathode half-cell using the polymer electrolyte separator membrane 5/95. Current rate: 0.2 C. Room temperature.

b and d), obtained at different current rates (i.e., from 0.1 C through 2 C), for Li/Sn–C (panels a and b) and Li/$LiFePO_4$ (panels c and d) half-cells. As expected, a progressive increase of the discharge plateau slope as well as the ohmic drop is observed with increasing the current density (panels a and c). The results depicted in panels b and d, and also summarized in Table 3, indicates that the half-cells are able to deliver appreciable capacity values up to a current rate of 0.5 C, e.g., more than 85% and 50% of the initial capacity are discharged at 0.2 C and 0.5 C, respectively (Table 3), this representing a remarkable value considering the gel configuration of the membrane. Higher current rates, i.e., 1 C and 2 C, result in modest delivered capacity values (Table 3), most likely limited by the polarization associated by the electrolyte diffusion kinetics. However, following cycling tests run again at 0.1 C have evidenced capacities close to the initial value (panels b and d), this clearly indicating good capacity uptake for both anode and the cathode cells. This behavior is also evidenced in Fig. 8, which displays the delivered capacity, normalized with respect to the nominal one, vs. current rate dependence. A progressive, almost linear, decrease in capacity is observed with increasing the current density up to 1 C, associated to diffusion phenomena taking place within the electrode active material phase and polymer electrolyte separator membrane. Further rise in the current rate above 1 C results just in modest capacity decay. This behavior can be ascribable to the intercalation of the Li^+ ion present in the electrode pores only. Nominally, no contribution from the Li^+ ion diffusion in the bulk electrolyte exists in this current regime.

Table 3
Room temperature specific capacity values delivered, at different current rates, by Li/Sn–C and Li/$LiFePO_4$ half-cells based on the P(VdF–HFP) 5/95 polymer electrolyte separator membrane.

Half-cell	Delivered capacity (mA h g^{-1})				
	0.1 C	0.2 C	0.5 C	1 C	2 C
Li/Sn–C	362.8	319.1	188.9	52.2	24.7
Li/$LiFePO_4$	122.1	105.8	66.9	3.9	0.05

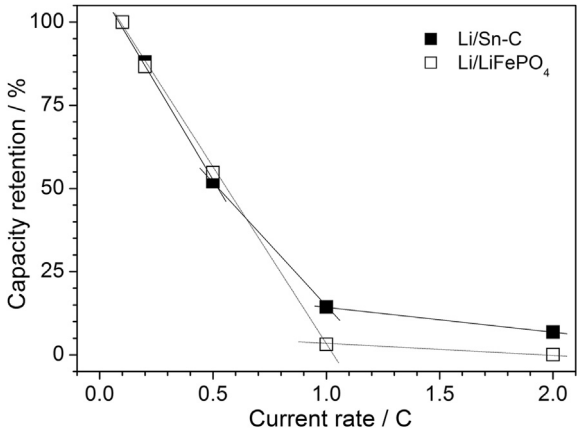

Fig. 8. Delivered capacity, normalized with respect to the nominal one, vs. current rate dependence for Li/Sn–C and Li/$LiFePO_4$ half-cells using the polymer electrolyte separator membrane 5/95. Room temperature.

4. Conclusions

The physicochemical properties of polymer electrolyte membranes, based on the P(VdF–HFP) copolymer and prepared through different polymer/solvent (DMF) ratios, as separators for lithium battery systems, were investigated.

SEM results have shown that optimally distributed porosity membranes with moderately tortuous pathways can be obtained from polymer/DMF slurries with a solvent content equal to or above 90% in weight. The P(VdF–HFP) samples were found able to retain liquid solution up to a fraction equal to 77% in weight. Impedance

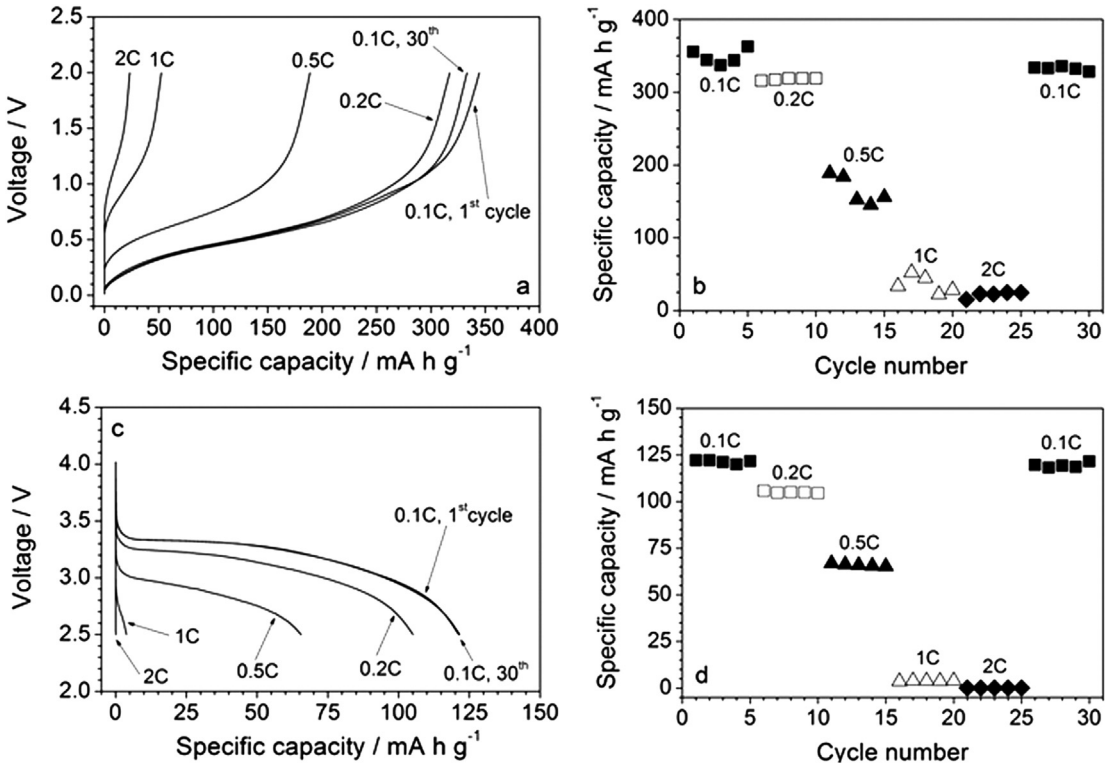

Fig. 7. Voltage vs. capacity profiles (panels a and c) and capacity evolution (panels b and d), obtained at different current rates (from 0.1 C through 2 C), for Li/Sn–C (panels a and b) and Li/$LiFePO_4$ (panels c and d) half-cells using the polymer electrolyte separator membrane 5/95. Room temperature.

measurements revealed conduction values above 10^{-3} S cm^{-1} at room temperature.

Cycling tests, performed on Li/Sn–C and Li/$LiFePO_4$ half-cells based on P(VdF–HFP) polymer electrolyte membranes, have evidenced nominal capacities ranging from 70% to 90% of the theoretical value with very good capacity retention and charge/discharge efficiency close at 100% even at high current rates and 100% of DOD. A capacity decay is observed at current regime above 1 C, associated to the diffusion phenomena taking place within the electrode active material phase and polymer electrolyte membrane. Further work is in progress for enhancing the rate capability especially at high rates, e.g., improving the pore distribution and interconnection within the separator membranes.

To summarize, the good cycling behavior exhibited by the half-cell indicates that the P(VdF–HFP) polymer electrolyte membranes developed in this work may be used as separators in lithium cell both in the anodic and in the cathodic region.

Acknowledgments

This work is funded by Federación Española de Enfermedades Raras funds through the "Programa Operacional Factores de Competitividade–COMPETE" and by national funds from FCT–Fundação para a Ciência e a Tecnologia, in the framework of the strategic project Strategic Project PEST-C/FIS/UI607/2011 and PEst-C/QUI/UI0686/2011. The authors also thank funding from Matepro-Optimizing Materials and Processes, ref. NORTE-07-0124-FEDER-000037, co-funded by the "Programa Operacional Regional do Norte" (ON.2 – O Novo Norte), under the "Quadro de Referência Estratégico Nacional" (QREN), through the "Fundo Europeu de Desenvolvimento Regional" (FEDER), and grants SFRH/BD/66930/2009 (J.N.P.) and SFRH/BD/68499/2010 (C.M.C.). G.B.A. thank the Italian Institute of Technology for the financial support. The authors thank Solvay for kindly supplying the high quality materials.

References

[1] Y. Ding, P. Zhang, Z. Long, Y. Jiang, F. Xu, W. Di, J. Membr. Sci. 329 (1–2) (2009) 56.
[2] P.G. Bruce, B. Scrosati, J.-M. Tarascon, Angew. Chem. Int. Ed. 47 (16) (2008) 2930.
[3] V. Aravindan, P. Vickraman, A. Sivashanmugam, R. Thirunakaran, S. Gopukumar, Curr. Appl. Phys. 13 (1) (2013) 293.
[4] X. Huang, J. Solid State Electrochem. 15 (2011) 649.
[5] H.-S. Kim, P. Periasamy, S.-I. Moon, J. Power Sources 141 (2) (2005) 293.
[6] L.N. Sim, S.R. Majid, A.K. Arof, Vibrat. Spectr. 58 (0) (2012) 57.
[7] D.-W. Kim, K.A. Noh, J.-H. Chun, S.-H. Kim, J.-M. Ko, Solid State Ionics 144 (3–4) (2001) 329.
[8] R. Miao, B. Liu, Z. Zhu, Y. Liu, J. Li, X. Wang, Q. Li, J. Power Sources 184 (2) (2008) 420.
[9] P. Martins, A.C. Lopes, S. Lanceros-Mendez, Progress Polym. Sci. 39 (4) (2014) 683–706.
[10] L. Shi, R. Wang, Y. Cao, C. Feng, D.T. Liang, J.H. Tay, J. Membr. Sci. 305 (1–2) (2007) 215.
[11] M.J. Koh, H.Y. Hwang, D.J. Kim, H.J. Kim, Y.T. Hong, S.Y. Nam, J. Mater. Sci. Tech. 26 (7) (2010) 633.
[12] J.-H. Cao, B.-K. Zhu, Y.-Y. Xu, J. Membr. Sci. 281 (1–2) (2006) 446.
[13] G.G. Kumar, K.S. Nahm, R.N. Elizabeth, J. Membr. Sci. 325 (1) (2008) 117.
[14] K. Smolders, A.C.M. Franken, Desalination 72 (3) (1989) 249.
[15] J. Hassoun, G. Derrien, S. Panero, B. Scrosati, Adv. Mater. 20 (2008) 3169.
[16] J. Hassoun, D.-J. Lee, Y.-K. Sun, B. Scrosati, Solid State Ionics 202 (1) (2011) 36.
[17] S. Brutti, J. Hassoun, B. Scrosati, C.-Y. Lin, H. Wu, H.-W. Hsieh, J. Power Sources 217 (2012) 72.
[18] G.A. Elia, S. Panero, A. Savoini, B. Scrosati, J. Hassoun, Electrochim. Acta 90 (2013) 690.
[19] A. California, V.F. Cardoso, C.M. Costa, V. Sencadas, G. Botelho, J.L. Gómez-Ribelles, S. Lanceros-Mendez, Eur. Polym. J. 47 (12) (2011) 2442.
[20] A. Ferreira, J. Silva, V. Sencadas, J.L.G. Ribelles, S. Lanceros-Méndez, Macromol. Mater. Eng. 295 (6) (2010) 523.
[21] C.M. Costa, M.M. Silva, S. Lanceros-Mendez, RSC Adv. 3 (2013) 11404.
[22] N. Ataollahi, A. Ahmad, H. Hamzah, M.Y.A. Rahman, N.S. Mohamed, Int. J. Electrochem. Sci. 7 (2012) 6693.
[23] D. Kumar, M. Suleman, S.A. Hashmi, Solid State Ionics 202 (2011) 45.
[24] J.R. MacDonald, Impedance Spectroscopy, John Wiley & Sons, New York, 1987.
[25] B.-Y. Chang, S.-M. Park, Annu. Rev. Anal. Chem. 3 (1) (2010) 207–229.
[26] B.A. Boukamp, Solid State Ionics 18 (1986) 136.
[27] B.A. Boukamp, Solid State Ionics 20 (1986) 31.
[28] G.B. Appetecchi, P. Romagnoli, B. Scrosati, Electrochem. Comm. 3 (2001) 281.
[29] Y. Aihara, G.B. Appetecchi, B. Scrosati, J. Electrochem. Soc. 149 (2002) A849.
[30] C.M. Costa, J.L. Gomez Ribelles, S. Lanceros-Méndez, G.B. Appetecchi, B. Scrosati, J. Power Sources 245 (2014) 779.
[31] Q. Shi, M. Yu, X. Zhou, Y. Yan, C. Wan, J. Power Sources 103 (2002) 286.
[32] S.S. Zhang, K. Xu, D.L. Foster, M.H. Ervin, T.R. Jow, J. Power Sources 125 (2004) 114.
[33] W. Pu, X. He, L. Wang, C. Jiang, C. Wan, J. Membr. Sci. 272 (2006) 11.
[34] D. Aurbach, J. Power Sources 89 (2) (2000) 206.
[35] J. Hassoun, K.-S. Lee, Y.-K. Sun, B. Scrosati, J. Am. Chem. Soc. 133 (9) (2011) 3139.
[36] B. Scrosati, Electrochim. Acta 45 (15–16) (2000) 2461.